

New structural anomaly induced by nanoconfinement

Leandro B. Krott*

*Programa de Pós-Graduação em Física, Instituto de Física,
Universidade Federal do Rio Grande do Sul,
Caixa Postal 15051, CEP 91501-970, Porto Alegre, RS, Brazil*

José Rafael Bordin[†]

*Campus Caçapava do Sul, Universidade Federal do Pampa,
Av. Pedro Anunciação, s/n, CEP 96570-000, Caçapava do Sul, RS, Brazil*

Marcia C. Barbosa[‡]

*Instituto de Física, Universidade Federal do Rio Grande do Sul,
Caixa Postal 15051, CEP 91501-970, Porto Alegre, RS, Brazil*

(Dated: October 22, 2014)

Abstract

We explore the structural properties of anomalous fluids confined in a nanopore using Molecular Dynamics simulations. The fluid is modeled by core-softened (CS) potentials that have a repulsive shoulder and an attractive well at a further distance. Changing the attractive well depth of the fluid-fluid interaction potential, we studied the behavior of the anomalies in the translational order parameter t and excess entropy s_{ex} for the particles near to the nanopore wall (contact layer) for systems with two or three layers of particles. When the attractive well of the CS potential is shallow, the systems present a three to two layers transition and, additionally to the usual structural anomaly, a new anomalous region in t and s_{ex} . For attractive well deep enough, the systems change from three layers to a bulk-like profile and just one region of anomaly in t and s_{ex} is observed. Our results are discussed in the basis of the fluid-fluid and fluid-surface interactions.

I. INTRODUCTION

Anomalous fluids exhibit a set of properties called anomalies that divert from the observed in simple fluids. The increase of density with the temperature at a fixed pressure and the increase of diffusivity under compression are examples of these anomalies. Water is the most well known fluid that present thermodynamic, dynamic and structural anomalous behavior¹⁻³, with 70 known anomalies⁴. In addition, Te^5 , Bi^6 , $\text{Si}^{7,8}$, $\text{Ge}_{15}\text{Te}_{85}^9$, liquid metals¹⁰, graphite¹¹, silica¹²⁻¹⁴, silicon¹⁵, BeF_2 ¹² exhibit thermodynamic anomalies³ while silica¹³⁻¹⁶ and silicon¹⁷ show a maximum in the diffusion coefficient at constant temperature, similar to what happens in water^{18,19}.

What these materials have in common that allow them to have anomalous properties? In order to answer to this question a measure of order of the liquid system was proposed^{13,20-22}. The translational order parameter,

$$t = \int |g(r) - 1| d^3r \quad (1)$$

measures the tendency of pairs of molecules to adopt a preferential separation. t vanishes for an ideal gas, and is large for a crystal. For normal liquids t increases with the increase with density, since the liquid becomes more ordered as it becomes more dense. In anomalous liquids there is a region in density in which t decreases with the increase of density. This decrease of structure with the increase in density indicates that the pairs of particles have two preferential separations: one more ordered in which particles are at further distance and another more disordered in which particles are closer²¹. As the density increases these bimodal distribution changes favoring the more disordered structure.

While t indicates through the structure the presence of the length scales the excess entropy²³⁻²⁶ gives a thermodynamic measure of the presence of anomalies in liquids²⁷. The excess entropy is defined as the difference between the entropy of a real fluid and that of an ideal gas at the same temperature and density, namely $s_{ex} = s - s_{ig}$. In principle the ideal entropy is $s_{ig} = \ln \rho + f(T)$ where $f(T)$ is a function of the temperature only. In the limit of $\rho \rightarrow \infty$, $s_{ex} \rightarrow 0_-$. For normal liquids as the density increases, s_{ex} decreases. The anomalous materials described above are characterized for having a region in density in which $(\partial s_{ex} / \partial \ln \rho) > 0$ ^{21,27}. This unusual behavior of s_{ex} is also related to the presence of two length scales²⁷. Even though t is related with the structure while s_{ex} to the thermodynamics these two quantities are in fact related. This becomes clear if the two body

approximation for s_{ex} namely

$$s_2 = \rho \int [g(r) \ln g(r) - g(r) + 1] d^3r \quad (2)$$

is employed. From the definitions of s_2 and t , both of which depend on deviations of $g(r)$ from unity, it is to be expected that variations in s_2 and t would be anticorrelated. Thus, the existence of a maximum in s_2 at high densities implies a minimum in t as a function of density. These two quantities connect the thermodynamic and structure by the two length scales.

Notwithstanding the relevance of the thermodynamic and dynamic anomalous bulk properties of the systems above, novel developments had arisen in the confined structures²⁸. In confined systems, crystallization is not uniform and depends on the size of the nanopores^{29,30}. Simulations for SPC/E water, for example, show partial crystallization inside nanotubes that leads to phase transitions not observed in bulk system^{31,32}. A transition between a bilayer ice and a trilayer fluid for different degrees of confinement also are observed for water^{33,34}. Under high degrees of confinement, water can form a monolayer ice and behaves very different from bulk systems^{35,36}, similar to what happens with two-dimensional core-softened fluids³⁷⁻³⁹. For confined systems, some anomalous liquids also present layering transition⁴⁰, superflow⁴¹⁻⁴⁴ and distinct dynamic behavior⁴⁵⁻⁴⁷. Oscillations in the solvation force⁴⁸ and a dramatic increase of the viscosity can occur in ultrathin confined fluids⁴⁹.

What does drive these novel phenomena observed in nanoconfined anomalous fluids? Under confinement, anomalous fluids exhibit properties not observed in bulk^{29-31,50-53}. The confined fluid is not distributed uniformly in the nanopore but forms layers. Therefore, the new anomalous properties that arise under confinement are related to the presence and structure of the layers. For instance, each layer might crystallize at a different temperature⁵⁴. Also the number of layers and their structures depend on the nanopore size and structure and on the fluid-wall interaction potential^{46,47}. Acknowledging that the presence of the layering structure is responsible for the novel behavior observed in anomalous fluids under confinement it is reasonable to think that the new properties appear as the result of the competition between the two fluid-fluid length scales and the fluid-wall length scale.

In order to check this hypothesis, in this paper we explore the behavior of the translational order parameter, t , and the excess entropy, s_{ex} , as a function of density and temperature of a confined model system of particle interacting through a core-softened potential. This two

length scales coarse-grained potential in the bulk exhibits the density, the diffusion and the structural anomalies^{55–57} observed in the water-like systems listed above. Under confinement this potential shows the formation of layers^{43–47,54}. Here we test for different ratios between the two fluid-fluid length scales if the presence of new anomalies in t and in s_{ex} are associated with changes in the layering structure. Our results give support to the surmise that the anomalies appear as the result of competition between bonding, nonbonding, hydrophilic and hydrophobic interactions.

The paper is organized as follows: in Sec. II we introduce the model and describe the methods and simulation details; the results are given and discussed in Sec. III; and in Sec. IV we present our conclusions.

II. THE MODEL AND THE SIMULATION DETAILS

A. The Model

The anomalous fluid was modeled using an isotropic effective potential⁵⁷ given by

$$\frac{U(r_{ij})}{\varepsilon} = 4 \left[\left(\frac{\sigma}{r_{ij}} \right)^{12} - \left(\frac{\sigma}{r_{ij}} \right)^6 \right] + a \exp \left[-\frac{1}{c^2} \left(\frac{r_{ij} - r_0}{\sigma} \right)^2 \right] - b \exp \left[-\frac{1}{d^2} \left(\frac{r_{ij} - r_1}{\sigma} \right)^2 \right],$$

where $r_{ij} = |\vec{r}_i - \vec{r}_j|$ is the distance between the two fluid particles i and j . The first term of this equation is a standard 12-6 Lennard-Jones (LJ) potential⁵⁸. The second and third terms are Gaussians centered at r_0 and r_1 , with depth a and b and width c and d , respectively. The fixed parameters of Eq. (3) are: $a = 5.0$, $r_0/\sigma = 0.7$, $c = 1.0$, $r_1/\sigma = 3.0$ and $d = 0.5$. Changing the parameter b , the attractive part increases without change the repulsive shoulder at $r \approx 1.2$. For $b = 0$ the potential is purely repulsive and presents density, diffusion and structural anomalies in bulk^{55,56} and in confined systems^{40,43–47,54}. Increasing b , beyond these anomalies, gas-liquid and liquid-liquid critical points appear in bulk systems⁵⁷. Besides $b = 0$ (model A), the potentials studied correspond to $b = 0.25$ (B), 0.50 (C) and 0.75 (D), as illustrated in Fig. 1 (a).

All these potentials are characterized by two length scales: one at the shoulder distance and another at the minimum of the potential. These two length scales can be seen more explicitly in the bulk radial distribution function that exhibits two peaks at these two rep-

representative distances⁵⁶ as illustrated in Fig. 2.

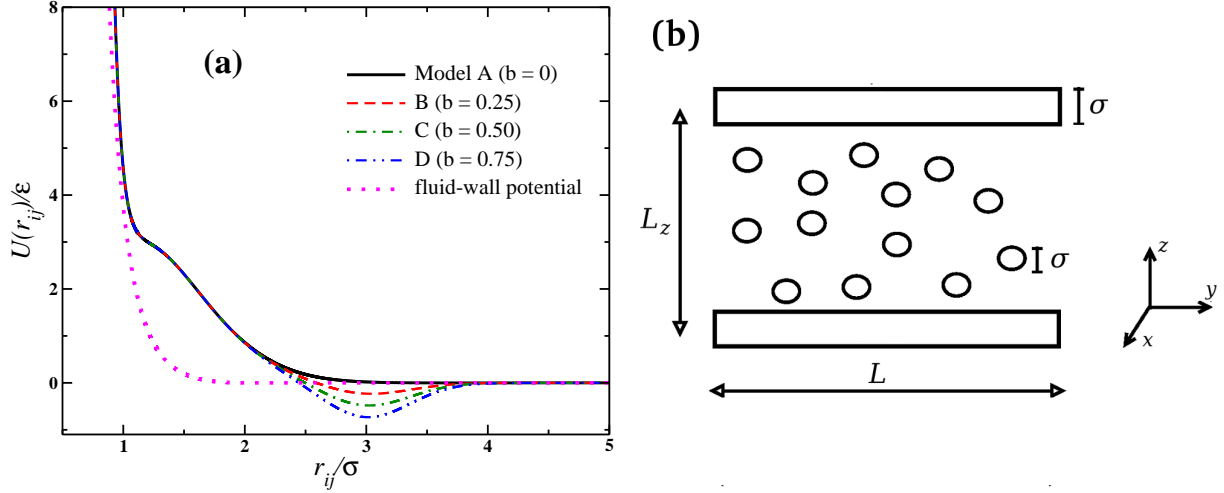


FIG. 1. (a) Particle-particle interaction potentials given by Eq. (3) with parameters $a = 5.0$, $r_0/\sigma = 0.7$, $c = 1.0$, $r_1/\sigma = 3.0$ and $d = 0.5$, for different values of b . (b) Schematic depiction of the fluid confined between two smooth walls.

In all cases the system was composed by N spherical particles of diameter σ and mass m confined between two smooth fixed walls, or plates, with area L^2 . The center-to-center plates distance is L_z . A schematic depiction of the system is shown in Fig. 1 (b). The particle-wall interaction was given by the sixth power (R6) potential⁵⁴,

$$U_{R6} = \begin{cases} 4\epsilon (\sigma/z_{ij})^6 + 0.1875\epsilon (z_{ij}/\sigma) - U_{R6c}, & z_{ij} \leq z_{cw} \\ 0, & z_{ij} > z_{cw} \end{cases} \quad (3)$$

where $z_{cw} = 2.0\sigma$ and $U_{R6c} = 4\epsilon (\sigma/z_{cw})^6 + 0.1875\epsilon (z_{cw}/\sigma)$. The term z_{ij} measures the distance between the wall at j position and the z -coordinate of the fluid particle i . This potential represents a hydrophobic nanopore-fluid interaction.

B. The simulation details

The simulations were performed in the NVT ensemble considering $N = 507$ particles. The plates have fixed positions and the distances between them was varied from $L_z = 5.3\sigma$ to $L_z = 7.5\sigma$, depending on the model considered. For each system, at a fixed L_z , different densities were obtained changing the simulation box size in the x and y direction, L , and

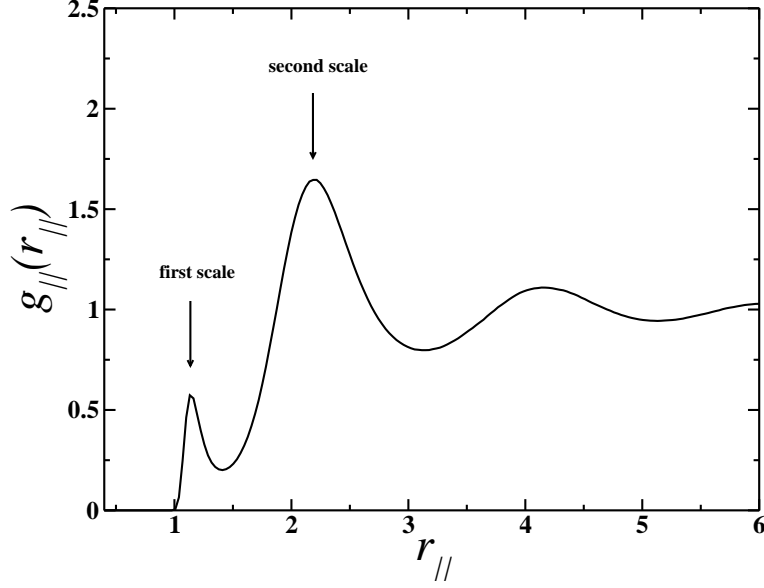


FIG. 2. Radial distribution function for potential Model A for the bulk system at $\rho = 0.137$ and $T = 0.175$. The two peaks represent the two fluid-fluid interaction length scales, as indicated by arrows.

consequently the plates size, from 20σ to 65σ . Standard periodic boundary conditions were applied in the x and y directions. Because of the excluded volume due the fluid-plate interaction, the distance L_z between the plates needs to be corrected to an effective distance^{59,60} that can be approached by $L_{ze} \approx L_z - \sigma$. The effective density will be $\rho_e = N/(L_{ze}L^2)$. The symbol e will be omitted in order to simplify the discussion.

The velocity Verlet algorithm was used to integrate the equations of motion for the fluid particles, considering a time step of $\delta t = 0.001$ in LJ units. We performed 4×10^5 steps to equilibrate the system and 8×10^5 steps to obtain the physical quantities. The temperature was kept fixed through the Nose-Hoover heat-bath with a coupling parameter $Q = 2$. The temperatures studied were different for each model considered: $k_B T/\varepsilon = 0.150, 0.250$ and 0.400 for the model A; $k_B T/\varepsilon = 0.200, 0.300$ and 0.500 for the model B; $k_B T/\varepsilon = 0.300$ and 0.500 for the model C; and $k_B T/\varepsilon = 0.500$ and 0.600 for the model D. The temperatures, densities and separation of plates were chosen according to the particularities of each model⁵⁷. The fluid-fluid interaction (Eq. (3)), has a cutoff radius $r_c/\sigma = 4.5$ for all models.

We analyze the structure of the system using the lateral radial distribution function $g_{||}(r_{||})$ and the translational order parameter, t . The $g_{||}(r_{||})$ is defined as

$$g_{\parallel}(r_{\parallel}) \equiv \frac{1}{\rho^2 V} \sum_{i \neq j} \delta(r - r_{ij}) [\theta(|z_i - z_j|) - \theta(|z_i - z_j| - \delta z)], \quad (4)$$

where the Heaviside function $\theta(x)$ restricts the sum of particle pair in a slab of thickness $\delta z = \sigma$ for the contact layer. The radial distribution function is proportional to the probability of finding a particle at a distance r from a referent particle.

The translational order parameter t is defined as^{13,21,22}

$$t \equiv \int_0^{\xi_c} |g_{\parallel}(\xi) - 1| d\xi, \quad (5)$$

where $\xi = r_{\parallel}(\rho^l)^{1/2}$ is the interparticle distance in the direction parallel to the plates scaled by the density of the layer, $\rho^l = N^l/L^2$. N^l is the average of particles for each layer. We use $\xi_c = (\rho^l)^{1/2}L/2$ as cutoff distance. The parameter t measures how structured is the system. For an ideal gas, $g(r) = 1$ and, consequently, $t = 0$, whereas for structured phases, like crystal and amorphous solids, t can assume large values.

The excess entropy is defined as the difference between the entropy of a real fluid and the ideal gas at the same temperature and density. As the systems are organized in layers of different structures, it is possible to define an excess entropy for each one, that can be approached as follows²³⁻²⁶

$$s_{ex} \approx -2\pi\rho^l \int_0^{\infty} [g_{\parallel}(r_{\parallel}) \ln g_{\parallel}(r_{\parallel}) - g_{\parallel}(r_{\parallel}) + 1] r_{\parallel}^2 dr_{\parallel}. \quad (6)$$

The physical quantities will be measured in the standard LJ units⁵⁸, namely

$$r^* \equiv \frac{r}{\sigma} \quad \text{and} \quad \rho^* \equiv \rho\sigma^3, \quad (7)$$

for distance and density of particles, respectively, and

$$T^* \equiv \frac{k_B T}{\epsilon} \quad \text{and} \quad s_{ex}^* \equiv \frac{s_{ex}}{k_B} \quad (8)$$

for temperature and excess entropy, respectively. Since all physical quantities are defined in reduced LJ units in this paper, the $*$ will be omitted, in order to simplify the discussion.

Data errors are smaller than the data points and are not shown. The data obtained in the equilibration period was not considered for the quantities evaluation.

III. RESULTS AND DISCUSSION

Usually fluids confined between flat plates are structured in layers. They can be classified in contact layers, which are in contact with the walls, and central layers, which are in the nanopore center without contact with the walls. The layer properties depend on the temperature, density and separation of the plates. In order to relate the fluid anomalies with the structure of the layers we have analyzed systems with two or three layers.

The Fig. 3 shows the transversal density profiles for each model. The Fig. 3(a) shows that at $T = 0.150$ potential A shows a transition from a regime of three layers at $L_z = 6.8$ and $\rho = 0.111$ to a regime of two layers for at $L_z = 5.3$ and $\rho = 0.150$. Fig. 3(b) shows a similar behavior for the potential B at $T = 0.200$ that exhibits three layers for 7.0 and $\rho = 0.108$ and two layers for $L_z = 5.7$ and $\rho = 0.137$. Fig. 3(c) for the potential C at $T = 0.300$ shows a different behavior. For both $L_z = 6.7$ with $\rho = 0.113$ and 7.5 with $\rho = 0.095$ between the two contact layers there is continuous distribution of particles forming an interlayer. Fig. 3(d) for the potential D at $T = 0.500$ shows also no transition when the confining distance changes from $L_z = 7.5$ and $\rho = 0.099$ to $L_z = 6.5$ and $\rho = 0.117$.

Figs. 3 show that in addition to the confining distance the well depth in Eq. (3) plays an important role in the number and structure of fluid layers. For the pure repulsive case, model A, the system shows distinct layers since particles in two different layers have no attraction. In addition the transition from two to three layers happens when a new layer can be accommodated satisfying the minimum of the fluid-fluid and wall-fluid energies. The model B, with a shallow well, shows a very similar behavior. On the other hand, for the cases with deep attractive well, models C and D, the system exhibits three not well defined layers for both plate separations. The central layer is present for distances between the confining walls that would imply that the fluid-fluid distance between particles in two neighbor layers is smaller than the minimum of the interparticle potential. The competition between the confinement and the fluid attraction leads to this scenario.

In order to test this in more detail in the next section the translational order parameter and the excess entropy will be analyzed for the four potentials.

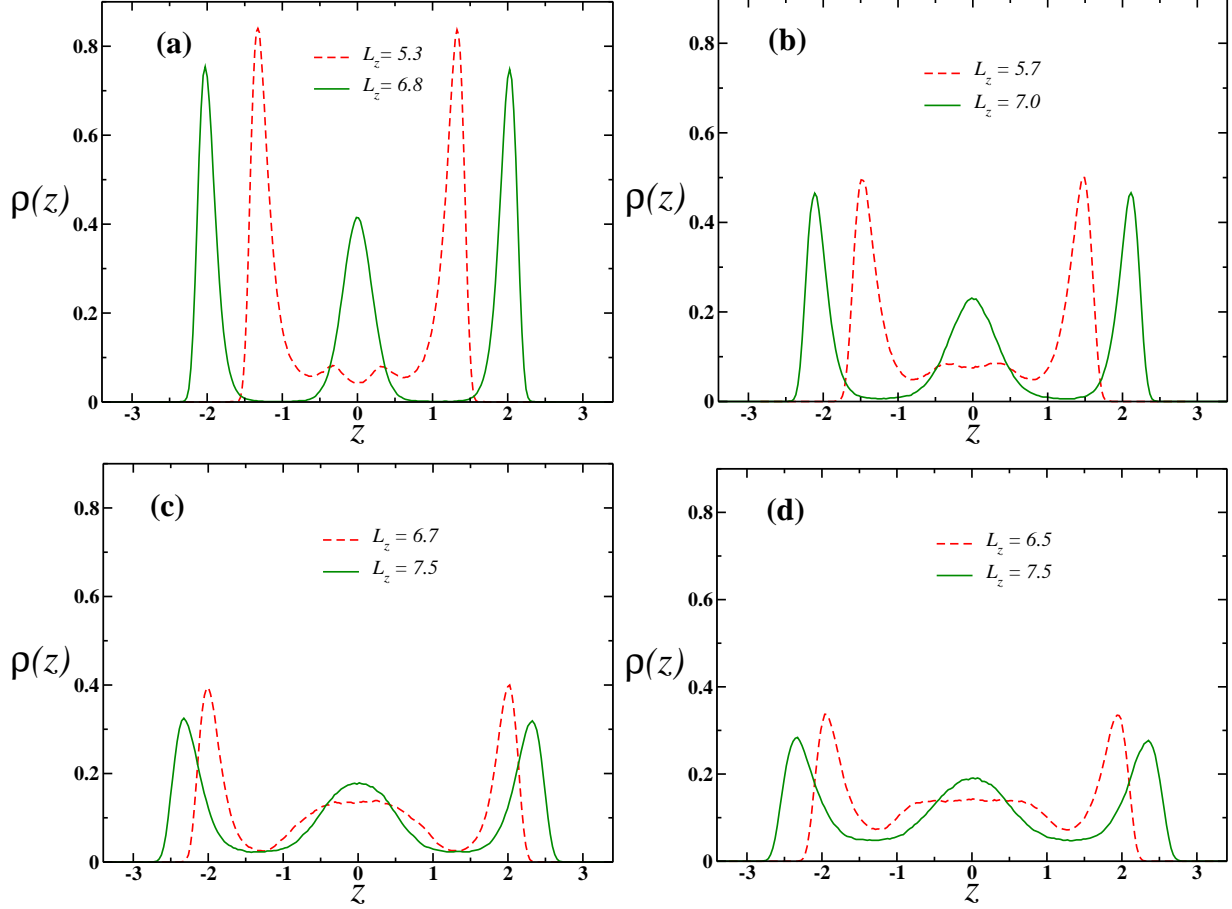


FIG. 3. Transversal density profiles for large and narrow systems at lowest temperature for (a) model A at $T = 0.150$, (b) model B at $T = 0.200$, (c) model C at $T = 0.300$ and (d) model D at $T = 0.500$. The correspondent densities for each case are given in the text.

Translational order parameter

The translational order parameter, t , was measured for the contact layer according to Eq. 5 for all the four models. Fig. 4 shows the parameter t as function of layer density ρ^l for (a) model A, (b) model B, (c) model C and (d) model D for fixed distances between the walls.

In normal fluids t increases monotonically with ρ for all temperatures, but anomalous fluids exhibit a region in the pressure versus temperature phase diagram in which t decreases with ρ leading to a density of maximum t at ρ_{tmax} and a density of minimum t at ρ_{tmin} . The interval of densities between $\rho_{tmax} < \rho < \rho_{tmin}$ defines the anomalous region in the pressure versus temperature phase diagram. The two densities, ρ_{tmax} and ρ_{tmin} , are associated with

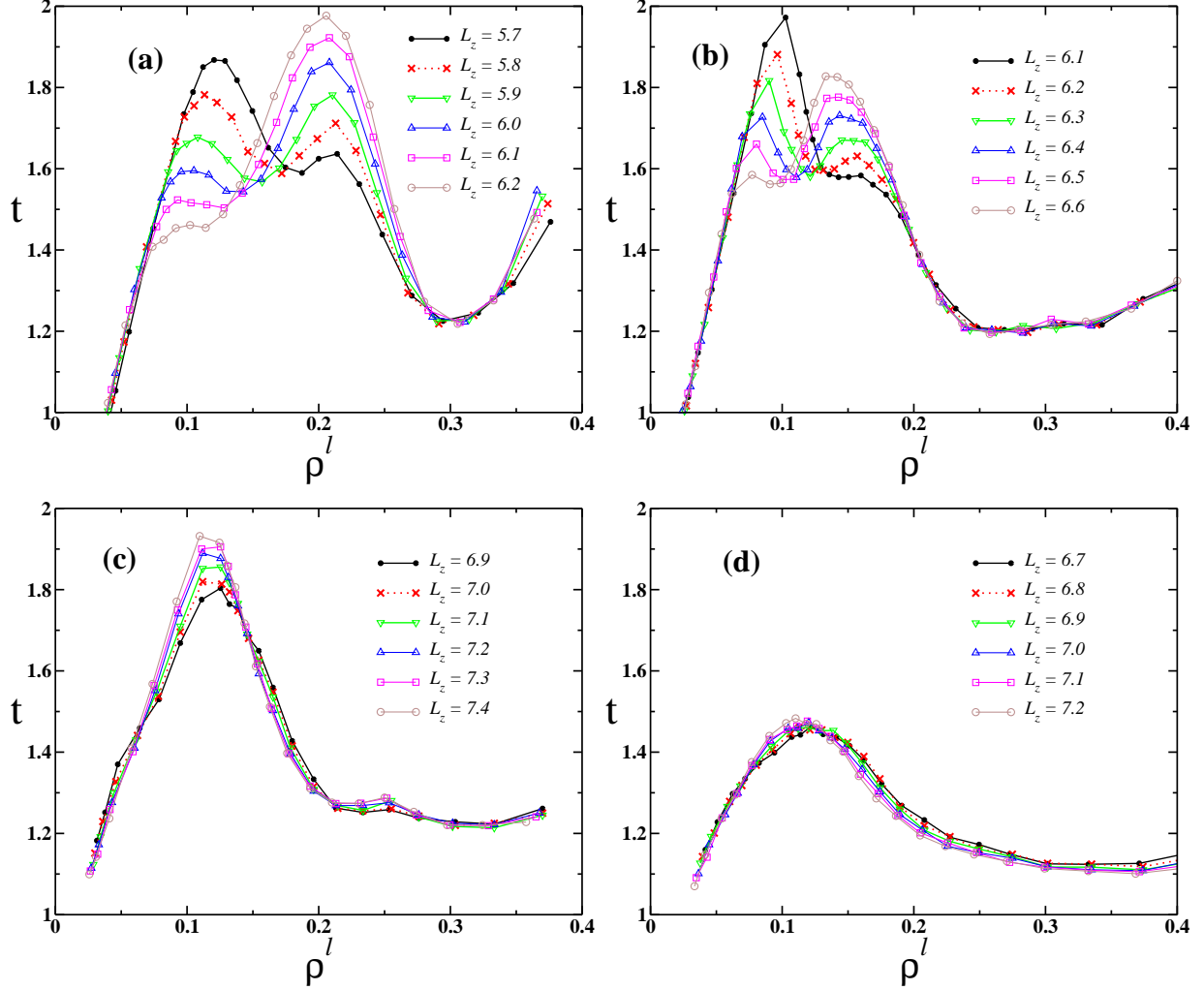


FIG. 4. Translational order parameter t as function of layer density for (a) model A at $T = 0.150$, (b) model B at $T = 0.200$, (c) model C at $T = 0.300$ and (d) model D at $T = 0.500$. The other temperatures and separation of plates were not shown for simplicity.

the two characteristic length scales of potential: one close to $r \approx 1.2$ and another at $r \approx 2.5$.

In the case of confined systems Fig. 4 (c) and (d) shows that the cases of the deepest attractive part, models C and D, exhibit the same anomalous behavior as the bulk with a layer density of maximum t , $\rho_{t_{max}}^l$, and a density of minimum t , $\rho_{t_{min}}^l$. The cases A and B, however, show an additional density of maximum t , $\rho_{t_{max1}}^l$, and density of minimum t , $\rho_{t_{min1}}^l$, that can not be associated with the two length scales of the bulk system.

Which mechanism leads to this new region of structural anomaly? In order to check if the new anomalous region is related to new structural arrangements not present in the

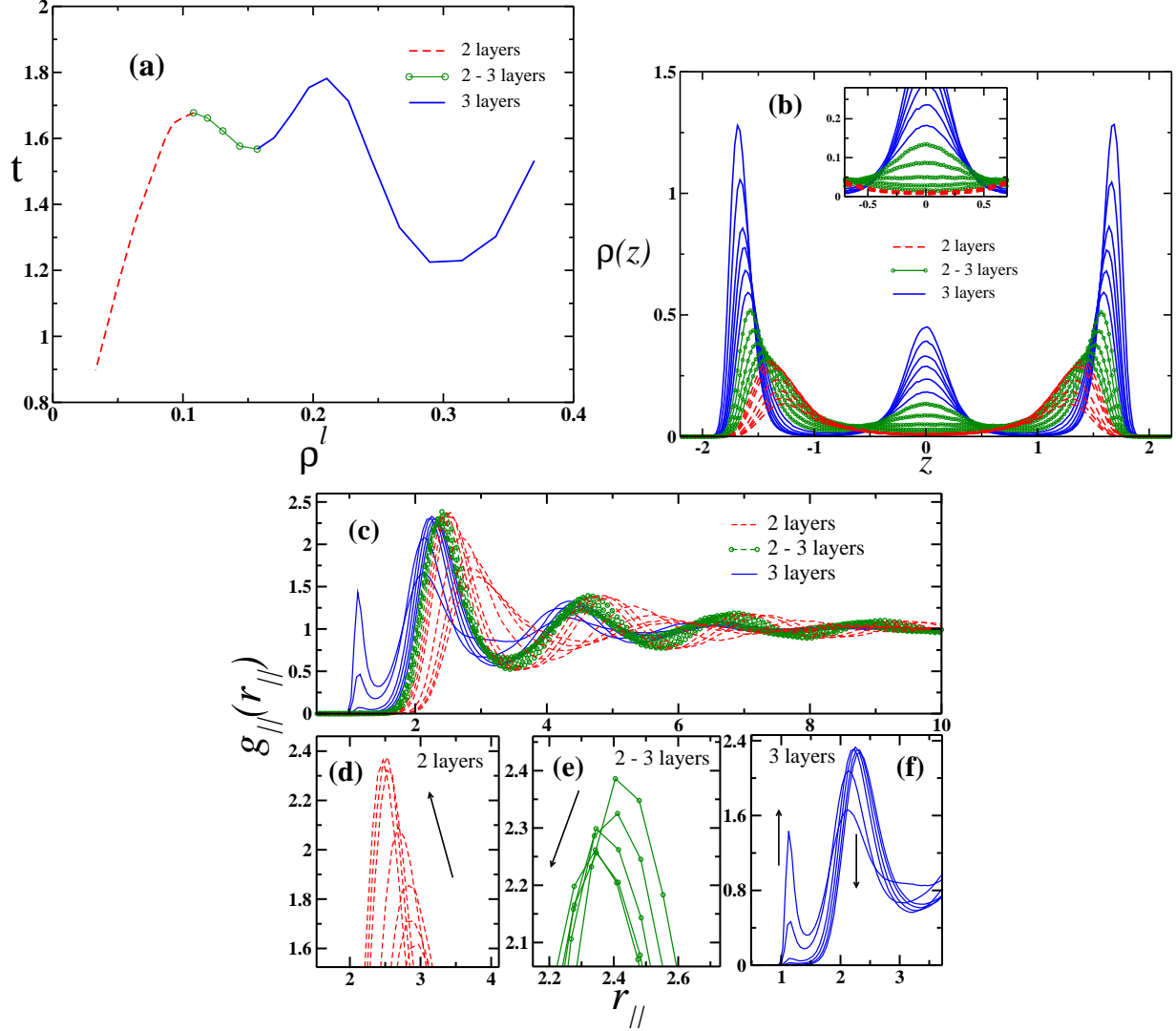


FIG. 5. Model A with plates separated by $L_z = 5.9$, temperature $T = 0.150$ and densities $\rho^l < 0.108$ (red dashed line), $0.108 \leq \rho^l \leq 0.157$ (green dotted line) and $\rho^l > 0.157$ (blue solid line). In (a) we have the translational order parameter as function of layer density, in (b) the transversal density profiles, in (c) the lateral radial distribution function (LRDF) versus lateral distance, in (d) and (e) a zoom of the first peak of the LRDF for systems with two layers and two to three layers, respectively, and in (f) the competition between scales in the LRDF for systems with three layers. The arrows indicate the increase of density.

bulk system, the densities of maximum and minimum t , ρ_{tmax}^l , ρ_{tmin}^l , ρ_{tmax}^l and ρ_{tmin}^l were inspected for number of layers.

Fig. 5 (a) shows the translational order parameter as function of layer density for plates separated for $L_z = 5.9$ and temperature $T = 0.150$. In addition to the expected minimum

of t in $\rho_{tmin}^l \approx 0.3$ (also observed in bulk system), a second minimum around $\rho_{tmin1}^l \approx 0.157$ appears. Likewise, besides the expected maximum, of t at $\rho_{tmax}^l \approx 0.2$, another maximum at $\rho_{tmax1}^l \approx 0.108$ appears.

The colors in the Fig. 5 (a) identify the number of layers in each region of the t versus contact layer density plot. Fig. 5 (b) shows that for high densities, $\rho^l > \rho_{tmin1}^l$ (blue curves), the system is ordered in three layers, while for low densities, $\rho^l < \rho_{tmax1}^l$ (red curves), shows just two well defined layers. The inset shows a zoom in the center of the plates illustrating that the new anomalous region in t happens for $\rho_{tmax1}^l < \rho^l < \rho_{tmin1}^l$, the region of densities where the system melts the central layer.

For the bulk system the peaks at the radial distribution function can be associated with the anomalous behavior of t and s_{ex} . For a fixed temperature two peaks associated with the two length scales of the potential at the $g(r)$ are present. As the density increases, the peak in the $g(r)$ associated with the smaller length scale, $r \approx 1.2$, increases while the larger peak, $r \approx 2.5$, decreases. The same phenomena can be seen for the lateral radial distribution function versus the lateral distance for $\rho^l > \rho_{tmin1}^l$ illustrated in Fig. 5 (c) (the blue plots) and Fig. 5 (f). This means that particles in all the three layers accommodate in arrangements in the two length scales. For low densities, $\rho^l < \rho_{tmax1}^l$, there is only a peak at the larger length scale and this peak increases with the increase of density as illustrated in Fig. 5 (c) (the red plots) and Fig. 5 (d) what is also observed in normal bulk systems. This implies that particles are arranged in the further length scale. For $\rho_{tmax1}^l < \rho^l < \rho_{tmin1}^l$ the behavior, shown in Fig. 5 (e), is different from the observed for bulk systems. The decrease in density implies an increase in the peak of the larger length scales because as the density is decreased the central layer melts and more particles are present in the contact layer, increasing the number of particles at the further length scale. The particular density in which the transition happens is related to the confining distance imposed by the wall-fluid interaction and the minimum of the fluid-fluid potential.

The structure of the model A also was analyzed for high temperatures, where the fluid shown only one region of structural anomaly. The Fig. 6 (a) shows the translational order parameter as function of layer density for plates separated by $L_z = 5.9$ and temperature $T = 0.400$. As we can see, for high temperatures, the higher entropic contribution for the fluid free energy leads the new structural anomaly to disappear. It occurs since the system changes from three layers at high densities to a bulk-like profile at low densities, like shown

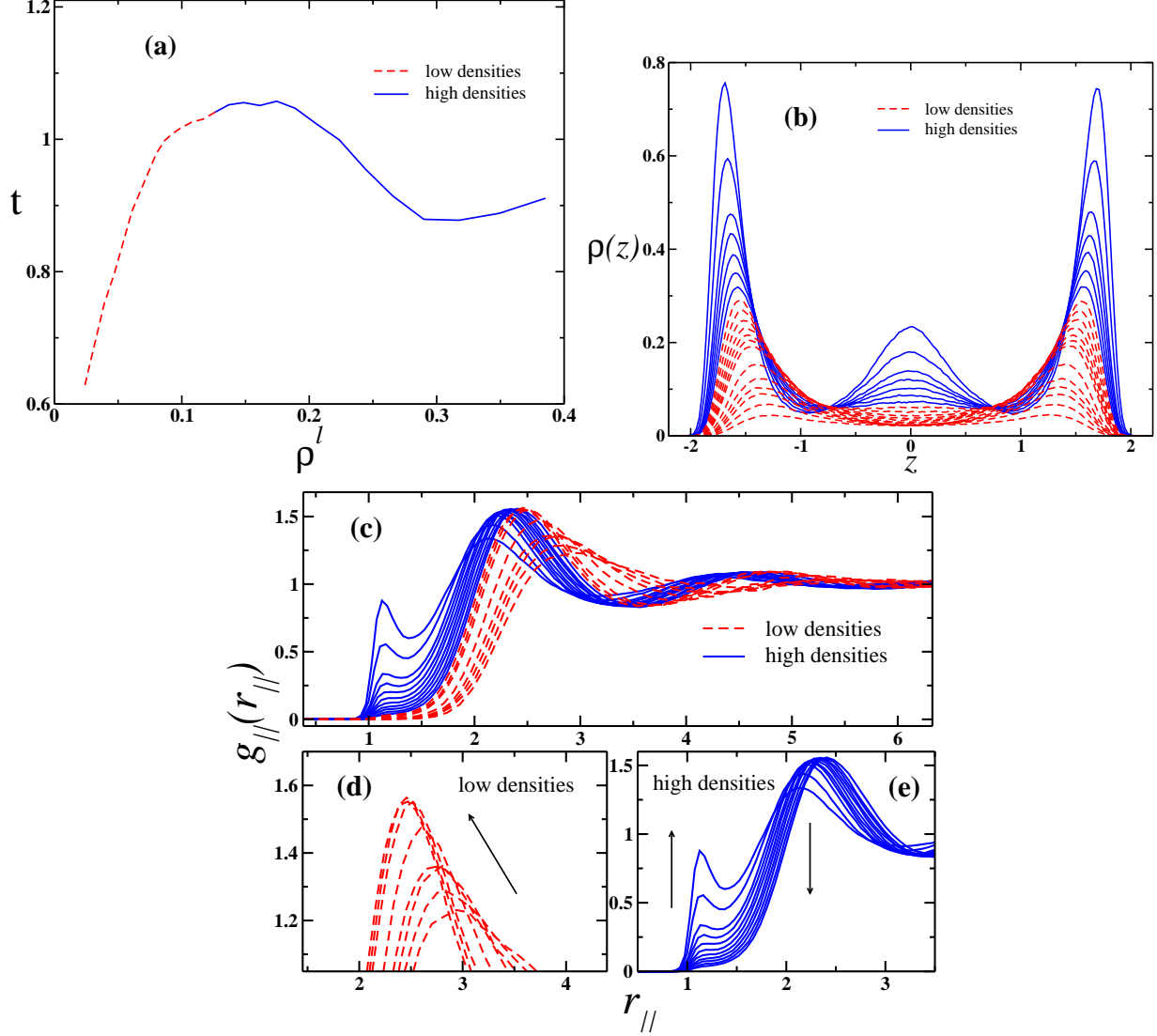


FIG. 6. Model A with plates separated by $L_z = 5.9$, temperature $T = 0.400$ and densities $\rho^l < 0.127$ (red dashed line) and $\rho^l \geq 0.127$ (blue solid line). In (a) we have the translational order parameter, in (b) the transversal density profile, in (c) the lateral radial distribution function versus lateral distance, in (d) a zoom of the first peak of the LRDF for low densities and in (e) the competition between scales observed in the LRDF for high densities. The arrows indicate the increase of density.

in the transversal density profiles in Fig. 6 (b). Two well defined layers, like observed for very low densities at $T = 0.150$ was not observed here, for $T = 0.400$. The lateral radial distribution function versus lateral distance was analyzed in Fig. 6 (c). For low densities the system presents a bulk-like profile and the $g_{\parallel}(r_{\parallel})$ presents the first peak around $r_{\parallel} \approx 2.5$. A zoom of this first peak is shown in Fig. 6 (d). As the density increases, this first peak in

the $g_{||}(r_{||})$ increases, as indicated by the arrow, and consequently the parameter t increases. Whereas, for high densities, the first peak occurs at $r_{||} \approx 1.2$ and a competition between scales is observed (Fig. 6 (e)) and the anomalous behavior in t is detected. The two to three layers transition does not occur and, because that, the double region of structural anomaly is not present. The same behavior was observed for the model B in the cases of one or two anomalous region. For simplicity, this results are not shown.

In the case of more attractive fluid-fluid potentials the fluid-fluid interaction always wins against the wall-fluid interaction and a middle layer that minimizes the fluid-fluid interaction is always formed.

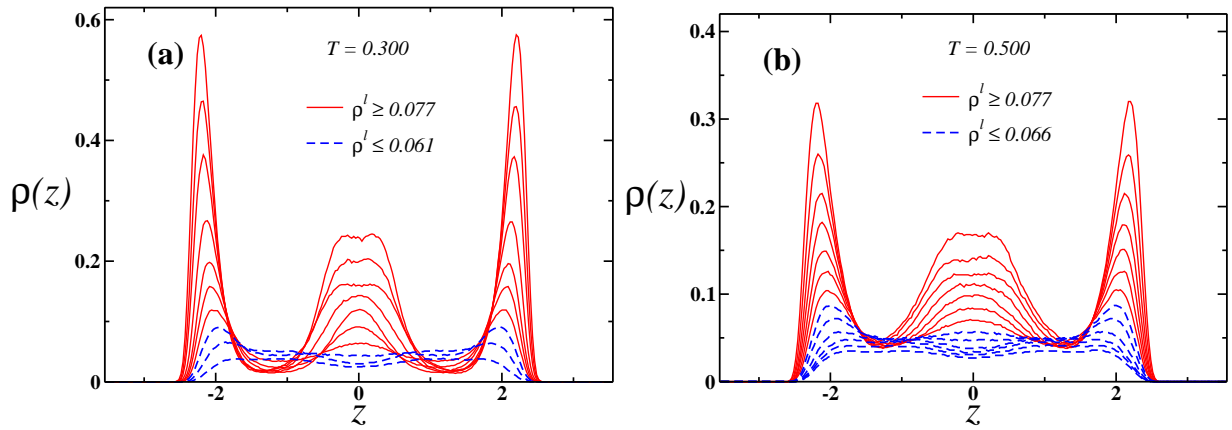


FIG. 7. Transversal density profile for (a) model C at $T = 0.300$ and (b) model D at $T = 0.500$. Both systems were simulated with plates separated by $L_z = 7.1$.

Fig. 7 (a) and (b) show the transversal density profiles for model C at $T = 0.300$ and model D at $T = 0.500$, respectively. In these models, the fluid changes from three layers of particles to a bulk-like profile regardless the system temperature. Therefore, the additional length that arises in models A and B is not present, and the second region of anomaly in t was not observed. The structural behavior for these models at low temperatures is similar to what happens with the models A and B for high temperatures.

The anomalous behavior in translational order parameter is a well known results for bulk systems^{13,20–22,27,61,62}. Similar to confined systems, Dudalov et al.^{37–39} analyzed the melting scenario of two-dimensional systems using structural order and found results very different from 3D cases. In the same way, our quasi-two-dimensional analysis also gives results completely different from the 3D bulk systems, arising the new anomaly caused by nanoconfinement.

Excess entropy

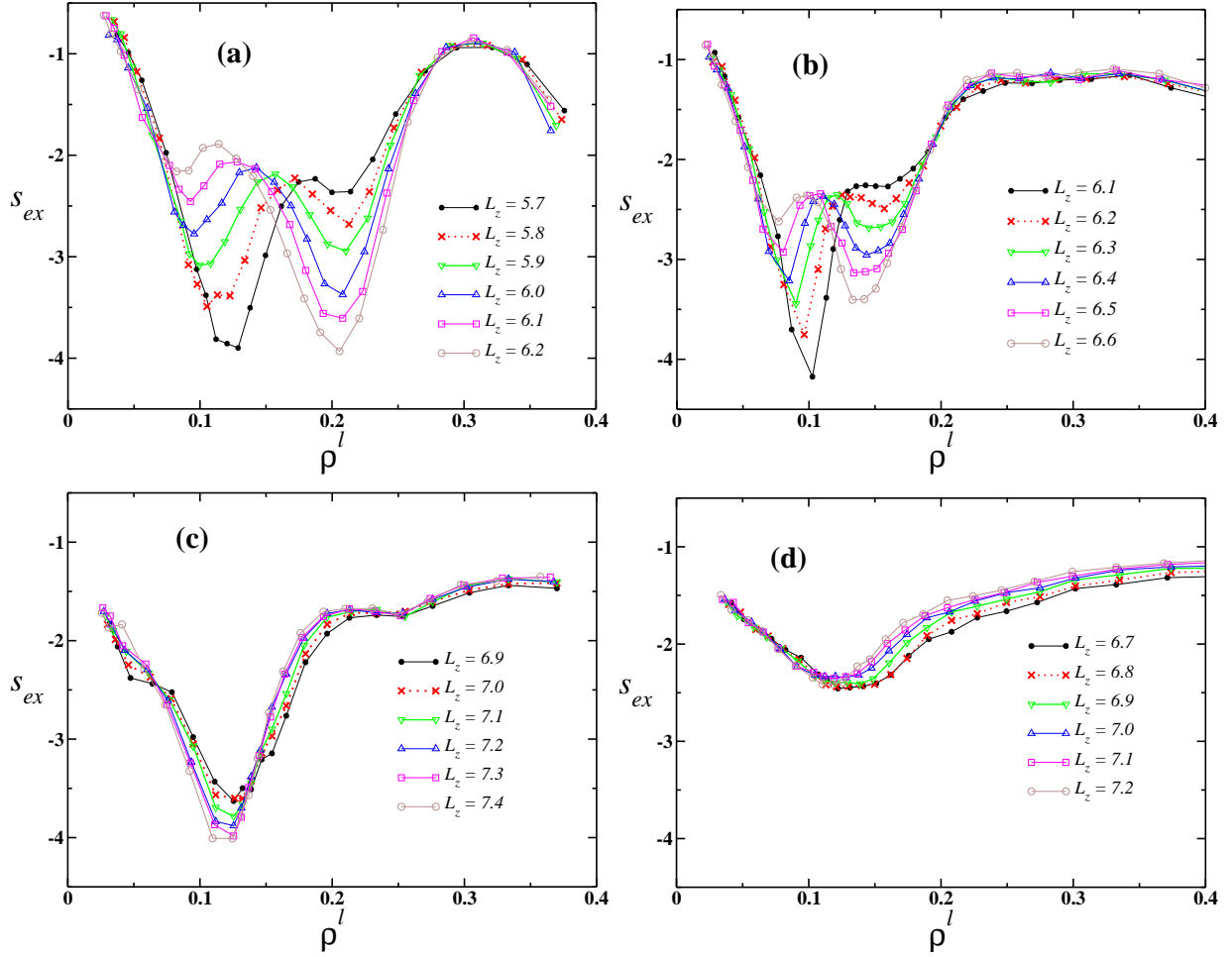


FIG. 8. Excess entropy as function of layer density for (a) model A at $T = 0.150$, (b) model B at $T = 0.200$, (c) model C at $T = 0.300$ and (d) model D at $T = 0.500$. The other temperatures and separation of plates were not shown for simplicity.

A second measure that relates the structure with the presence of anomalies is the excess entropy. In order to confirm that the presence of the new anomalous region in the structure is also related to anomalies in the thermodynamics, the excess entropy was computed for each of the models studied here. The models studied in this work in the bulk exhibit the anomalous increase of s_{ex} with the increase of density^{57,63}.

Fig. 8 shows the excess entropy for the contact layer as function of layer density ρ^l for (a) model A, (b) model B, (c) model C and (d) model D. The same behavior observed for the translational order parameter is seen for the excess entropy. For the models C and D the

same anomalous region in the excess entropy versus density phase diagram observed in bulk systems appears under confinement. However, the models A and B exhibit an additional region of anomaly for low temperatures and some distances L_z between plates.

The new region of anomaly in s_{ex} is shown in Fig. 9 (a) for the model A at $L_z = 5.9$ and $T = 0.150$ and (b) model B at $L_z = 6.3$ and $T = 0.200$. The densities of maxima and minima of excess entropy, $\rho_{sexmax1}^l, \rho_{sexmax}^l, \rho_{sexmin1}^l$ and ρ_{sexmin}^l , coincide with the densities of maxima and minima of translational order parameter. This shows that as the system changes from three to two layers the density of the contact layer increases, it becomes more structured and the entropy decreases what is a consistent picture. Similarly to what happens in the t behavior, as the temperature increases, the entropic effect leads the fluid to assume a bulk-like behavior and the new region of anomaly disappears.

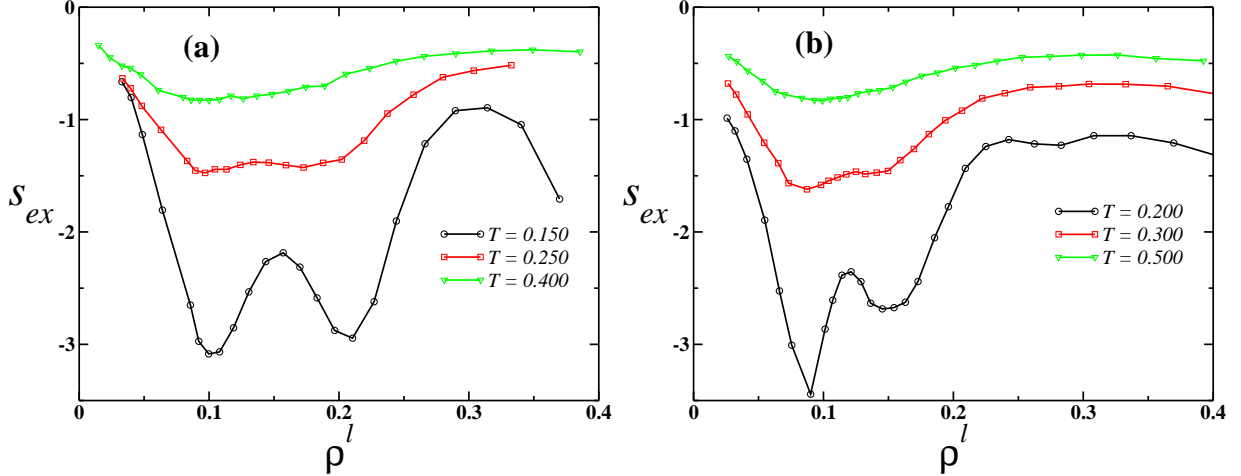


FIG. 9. Excess entropy for (a) model A at $L_z = 5.9$ and (b) model B at $L_z = 6.3$.

The excess entropy is a good tool to understand the dynamic of bulk and confined fluids^{64–67} and can be useful to see the presence of density anomaly as well^{26,27,68}. The increase of attractive well of core-softened models can destroy the water-like anomalies in bulk⁵⁷ and the second region of anomaly in t and s_{ex} in confinement by plates.

IV. CONCLUSION

In this work we have analyzed the effects of confinement in a system of particles interacting through models of two length scale potential, varying from a purely repulsive (model A) to models that have an attractive well (models B, C and D).

We found that the confinement in the case of systems in which the fluid-wall interaction competes with the fluid-fluid interaction potentials leads to the appearance of new anomalous region in the translational order parameter versus density phase diagram. This new anomalous behavior is related to the change of structure that happens when the system changes from three to two layers, namely when the center layer melts.

The same behavior is observed from the thermodynamic side by the excess entropy that increases with increasing density.

Our results indicates that by confining and particularly by confining by system with strong interacting walls the confined fluid exhibits new phenomena not observed in the bulk systems.

V. ACKNOWLEDGMENTS

We thanks the Brazilian agencies CNPq, INCT-FCx, and Capes for the financial support.

* leandro.krott@ufrgs.br

† josebordin@unipampa.edu.br

‡ marciabarbosa@ufrgs.br

¹ G. S. Kell, J. Chem. Eng. Data **20**, 97 (1975).

² C. A. Angell, E. D. Finch, and P. Bach, J. Chem. Phys. **65**, 3065 (1976).

³ F. X. Prielmeier, E. W. Lang, R. J. Speedy, and H.-D. Lüdemann, Phys. Rev. Lett. **59**, 1128 (1987).

⁴ M. Chaplin, Sixty-nine anomalies of water, <http://www.lsbu.ac.uk/water/anmlies.html>, 2013.

⁵ H. Thurn and J. Ruska, J. Non-Cryst. Solids **22**, 331 (1976).

⁶ *Handbook of Chemistry and Physics*, CRC Press, Boca Raton, Florida, 65 ed. edition edition, 1984.

⁷ G. E. Sauer and L. B. Borst, Science **158**, 1567 (1967).

⁸ S. J. Kennedy and J. C. Wheeler, J. Chem. Phys. **78**, 1523 (1983).

⁹ T. Tsuchiya, J. Phys. Soc. Jpn. **60**, 227 (1991).

- ¹⁰ P. T. Cummings and G. Stell, *Mol. Phys.* **43**, 1267 (1981).
- ¹¹ M. Togaya, *Phys. Rev. Lett.* **79**, 2474 (1997).
- ¹² C. A. Angell, R. D. Bressel, M. Hemmatti, E. J. Sare, and J. C. Tucker, *Phys. Chem. Chem. Phys.* **2**, 1559 (2000).
- ¹³ M. S. Shell, P. G. Debenedetti, and A. Z. Panagiotopoulos, *Phys. Rev. E* **66**, 011202 (2002).
- ¹⁴ R. Sharma, S. N. Chakraborty, and C. Chakravarty, *J. Chem. Phys.* **125**, 204501 (2006).
- ¹⁵ S. Sastry and C. A. Angell, *Nature Mater.* **2**, 739 (2003).
- ¹⁶ S.-H. Chen et al., *Proc. Natl. Acad. Sci. USA* **103**, 12974 (2006).
- ¹⁷ T. Morishita, *Phys. Rev. E* **72**, 021201 (2005).
- ¹⁸ P. A. Netz, F. W. Starr, H. E. Stanley, and M. C. Barbosa, *J. Chem. Phys.* **115**, 344 (2001).
- ¹⁹ P. A. Netz, F. W. Starr, M. C. Barbosa, and H. E. Stanley, *Physica A* **314**, 470 (2002).
- ²⁰ T. M. Truskett, S. Torquato, and P. G. Debenedetti, *Phys. Rev. E* **62**, 993 (2000).
- ²¹ J. R. Errington and P. D. Debenedetti, *Nature (London)* **409**, 318 (2001).
- ²² J. E. Errington, P. G. Debenedetti, and S. Torquato, *J. Chem. Phys.* **118**, 2256 (2003).
- ²³ R. E. Nettleton and H. S. Green, *J. Chem. Phys.* **29**, 1365 (1958).
- ²⁴ H. J. Raveché, *J. Chem. Phys.* **55**, 2242 (1971).
- ²⁵ D. C. Wallace, *J. Chem. Phys.* **87**, 2282 (1987).
- ²⁶ A. Baranyai and D. J. Evans, *Phys. Rev. A* **40**, 3817 (1989).
- ²⁷ J. R. Errington, T. M. Truskett, and J. Mittal, *J. Chem. Phys.* **125**, 244502 (2006).
- ²⁸ P. Tabeling and L. Bocquet, *Lab on a Chip* **14**, 3143 (2014).
- ²⁹ J. Deschamps, F. Audonnet, N. Brodie-Linder, M. Schoeffel, and C. Alba-Simionesco, *Phys. Chem. Chem. Phys.* **12**, 1440 (2010).
- ³⁰ S. Jähnert et al., *Phys. Chem. Chem. Phys.* **10**, 6039 (2008).
- ³¹ K. Koga, G. T. Gao, H. Tanaka, and X. C. Zeng, *Nature* **412**, 802 (2001).
- ³² M. W. Maddox and K. E. Gubbins, *J. Chem. Phys.* **107**, 9659 (1997).
- ³³ N. Giovambattista, P. J. Rossky, and P. G. Debenedetti, *Phys. Rev. Lett.* **102**, 050603 (2009).
- ³⁴ T. G. Lombardo, P. J. Rossky, and P. G. Debenedetti, *Faraday Discuss.* **141**, 359 (2009).
- ³⁵ R. Zangi and A. E. Mark, *Phys. Rev. Lett.* **91**, 025502 (2003).
- ³⁶ F. de los Santos and G. Franzese, *Phys. Rev. E* **85**, 010602 (2012).
- ³⁷ D. E. Dudalov, Y. D. Fomin, E. N. Tsiok, and V. N. Ryzhov, *Soft Matter* **10**, 4966 (2014).

- ³⁸ D. E. Dudalov, Y. D. Fomin, E. N. Tsiok, and V. N. Ryzhov, *Journal of Physics: Conference Series* **510**, 012016 (2014).
- ³⁹ D. E. Dudalov, Y. D. Fomin, E. N. Tsiok, and V. N. Ryzhov, *Physical Review Letters* **112**, 157803 (2014).
- ⁴⁰ J. R. Bordin, L. Krott, and M. C. Barbosa, *J. Phys. Chem. C* **118**, 9497 (2014).
- ⁴¹ S. Jakobtorweihen, M. G. Verbeek, C. P. Lowe, . F. J. Keil, and B. Smit, *Phys. Rev. Lett.* **95**, 044501 (2005).
- ⁴² X. Qin, Q. Yuan, Y. Zhao, S. Xie, and Z. Liu, *Nanoletters* **11**, 2173 (2011).
- ⁴³ J. R. Bordin, A. Diehl, and M. C. Barbosa, *J. Phys. Chem. B* **117**, 7047 (2013).
- ⁴⁴ J. R. Bordin, J. S. Soares, A. Diehl, and M. C. Barbosa, *J. Chem Phys.* **140**, 194504 (2014).
- ⁴⁵ L. Krott and J. R. Bordin, *J. Chem. Phys.* **139**, 154502 (2013).
- ⁴⁶ L. Krott and M. C. Barbosa, *J. Chem. Phys.* **138**, 084505 (2013).
- ⁴⁷ J. R. Bordin, A. B. de Oliveira, A. Diehl, and M. C. Barbosa, *J. Chem. Phys* **137**, 084504 (2012).
- ⁴⁸ R. G. Horn and J. N. Israelachvili, *J. Chem. Phys* **75**, 1400 (1981).
- ⁴⁹ S. Granick, *Science* **253**, 1374 (1991).
- ⁵⁰ K. Koga, X. C. Zeng, and H. Tanaka, *Phys. Rev. Lett.* **72**, 5262 (1997).
- ⁵¹ E. G. Strelakova, J. Luo, H. E. Stanley, G. Franzese, and S. V. Buldyrev, *Phys. Rev. Lett.* **109**, 105701 (2012).
- ⁵² A. Faraone, K.-H. Liu, C.-Y. Mou, Y. Zhang, and S.-H. Chen, *J. Chem. Phys.* **130**, 134512 (2009).
- ⁵³ M. Erko, N. Cade, A. G. Michette, G. H. Findenegg, and O. Paris, *Phys. Rev. B* **84**, 104205 (2011).
- ⁵⁴ L. Krott and M. C. Barbosa, *Phys. Rev. E* **89**, 012110 (2014).
- ⁵⁵ A. B. de Oliveira, P. A. Netz, T. Colla, and M. C. Barbosa, *J. Chem. Phys.* **124**, 084505 (2006).
- ⁵⁶ A. B. de Oliveira, P. A. Netz, T. Colla, and M. C. Barbosa, *J. Chem. Phys.* **125**, 124503 (2006).
- ⁵⁷ J. N. da Silva, E. Salcedo, A. B. de Oliveira, and M. C. Barbosa, *J. Chem. Phys.* **133**, 244506 (2010).
- ⁵⁸ P. Allen and D. J. Tildesley, *Computer Simulation of Liquids*, Oxford University Press, Oxford, 1987.

- ⁵⁹ P. Kumar, S. V. Buldyrev, F. Sciortino, E. Zaccarelli, and H. E. Stanley, Phys. Rev. E **72**, 021501 (2005).
- ⁶⁰ P. Kumar, F. W. Starr, S. V. Buldyrev, and H. E. Stanley, Phys. Rev. E **72**, 011202 (2007).
- ⁶¹ Z. Yan, S. V. Buldyrev, N. Giovambattista, and H. E. Stanley, Phys. Rev. Lett. **95**, 130604 (2005).
- ⁶² J. Mittal, J. R. Errington, and T. M. Truskett, J. Phys. Chem. B **110**, 18147 (2006).
- ⁶³ A. B. de Oliveira, E. Salcedo, C. Chakravarty, and M. C. Barbosa, J. Chem. Phys. **132**, 234509 (2010).
- ⁶⁴ R. Chopra, T. M. Truskett, and J. R. Errington, Phys. Rev. E **82**, 041201 (2010).
- ⁶⁵ B. J. Borah, P. K. Maiti, C. Chakravarty, and S. Yashonath, J. Chem. Phys. **136**, 174510 (2012).
- ⁶⁶ T. S. Ingebrigtsen, J. R. E. T. M. Truskett, and J. C. Dyre, Phys. Rev. Lett. **111**, 235901 (2013).
- ⁶⁷ M. Singh, H. Liu, S. K. Kumar, A. Ganguly, and C. Chakravarty, J. Chem. Phys. **132**, 074503 (2010).
- ⁶⁸ S. N. Chakraborty and C. Chakravarty, J. Chem. Phys. **124**, 014507 (2006).